JOURNAL OF GEOPHYSICAL RESEARCH, VOL. 103, NO. D11, PAGES 13,181–13,194, JUNE 20, 1998

Harvard Forest regional-scale air mass composition by Patterns in Atmospheric Transport History (PATH)

J. L. Moody,[1] J. W. Munger,[2] A. H. Goldstein,[3] D. J. Jacob,[2] and S. C.Wofsy[4]

Abstract. We calculated 4 years (1990-1993) of back trajectories arriving at Harvard Forest and used them to define patterns in atmospheric transport history. This information was used to assess the degree to which regional-scale transport modulates the chemical composition of air masses sampled at Harvard Forest. Different seasonal signals in trace-gas concentration are derived for different flow patterns. Throughout the year, high-speed transport of cool, dry, cloud-free air from the north and northwest represents background conditions for the Harvard Forest site. These synoptic conditions describe the atmosphere after passage of a cold front. The most polluted conditions in each season occurred under SW flow, with warmer temperatures, higher water vapor mixing ratios, low mixed-layer depths at the site, and a higher frequency of cloudy conditions. These regional-scale air mass characteristics describe synoptic conditions of warm sector transport. In addition to average air mass characteristics, we have analyzed the covariation of species (e.g., O_3 versus NO_y-NO_x; O_3 versus CO) to address chemical processes based on transport history. For summer daytime measurements, we show that relatively fresh pollutants arrive in SW flow while the most aged air masses with higher O_3 to NO_z slopes arrive with W flow, suggesting a Midwestern contribution to regional high-oxidant episodes. These observations of patterns in chemical characteristics related to patterns in transport are corroborated with probability maps indicating the likelihood of transport from upwind regions using trajectories selected for chemical distribution end-members (10^{th} and 90^{th} percentiles).

1. Introduction

The Harvard Forest measurement site in central Massachusetts is designed to provide long-term records of the concentrations of climatologically important trace gases in a rural area adjacent to heavily populated regions [*Munger et al.*, 1996]. Research activities at this Long Term Ecological Research (LTER) site are focused on improving our understanding of the effects of forests on gases like CO_2, CH_4, and O_3, as well as understanding the effects that anthropogenic changes in CO_2 and air pollution may have on forest resources [*Wofsy et al.*, 1993; *Goulden et al.*, 1996]. Trace gas concentrations currently measured at the tower site, 5 m above the canopy, are CO, CO_2, O_3, NO, NO_2, NO_y, and methane and nonmethane hydrocarbons [*Goldstein et al.*, 1995a,b]. The temporal variance in each species concentration record offers unique clues as to the origin of the species, including in particular the role of human influence. Interpreting this variance is, however, a challenging task. Changing meteorology is certainly a major factor contributing to the variance in atmospheric chemical composition, and some of this variability can be accounted for in a quantitative manner [*Moody et al.*, 1995]. In particular, it is possible to filter out the highly variable influence of regional-scale motion on the measured atmospheric concentrations of trace gases.

A recent paper by *Munger et al.* [1996] describes the synoptic scale variability in concentration and deposition of reactive nitrogen oxides and ozone at Harvard Forest and illustrates significant differences in concentration distributions after stratifying data on the basis of local wind direction. In this paper, we go beyond the local conditions and begin to assess the degree to which variation in regional-scale transport modulates the concentrations of chemically and radiatively important trace gases measured at Harvard Forest. Using back trajectories, distinct patterns of regional-scale transport to Harvard Forest have been identified, and the relative frequency of occurrence of flow from different upwind regions is presented. For each flow pattern, characteristic chemical signatures and trace gas ratios, and local meteorological conditions have been defined. Analysis of variance techniques have been used to compare the chemistry and meteorology of events with different regional-scale transport history. We show that regional-scale differences in airflow can explain a significant portion of the variability in chemical composition.

2. Methods

2.1. Trajectory Calculation

Trajectories were calculated back from Harvard Forest for three different starting times during the day, 1200, 1600, and

[1] Department of Environmental Sciences, University of Virginia, Charlottesville.
[2] Division of Applied Science, Harvard University, Cambridge, Massachusetts.
[3] Environmental Science, Policy, and Management, University of California, Berkeley.
[4] Northeast Regional Center, National Institute of Global Environmental Change, Harvard University, Cambridge, Massachusetts.

Paper number 98JD00526.
0148-0227/98/98JD-00526$09.00

2000 UTC, corresponding to 0700, 1100, and 1500 LST, respectively. The back trajectories for this project were calculated using the wind and temperature fields of the National Meteorological Center Nested Grid Model (MNC-NGM) [*Hoke et al.*, 1989]. The NGM provides assimilated observations combined with 12-hour forecast fields of high spatial and temporal resolution, and includes dynamically consistent vertical velocities at 10 terrain-following sigma levels between the surface and ~400 hPa. Using these model fields, and the HY-SPLIT trajectory code [*Draxler*, 1992] three-dimensional trajectories of air parcel transport were calculated back from Harvard Forest. To determine the height from which to start the trajectories, the depth of the surface mixed layer was determined from the NGM temperature profile, and the trajectories were initiated from this height in an effort to represent the origin of air parcels advected in the mixed layer. This meant we did not calculate trajectories for the same starting height every day. For example, on days with a surface-based temperature inversion, trajectories were initiated from the model's lowest sigma-level, while on other days, for example, in the well-mixed summer atmosphere behind a cold front, the top of the mixed layer was a few thousand meters above the surface. Table 1 illustrates the number of trajectories calculated by month, and the median mixed-layer height for the Harvard Forest NGM gridcell based on the NGM model potential temperature lapse rate. It shows the climatological seasonal variation of shallow mixed layers during the cool months, transitioning to the deepest mixed layers in summer months, when surface heating (represented here by ambient air temperature measured at Harvard Forest) is most significant. These observations are very similar to the seasonal variation in afternoon mixing depths over the eastern United States which *Holzworth* [1967] derived from morning radiosonde profiles and local surface temperatures. While this average condition may be climatologically expected, when we assess all the trajectories, there are significant differences in day to day mixed-layer depth driven by regional-scale weather patterns that may have a controlling influence on air mass chemical variability. These differences in mixed-layer depth and air mass origin are what we seek to describe with a pattern recognition analysis of back trajectories.

Table 1. Model Estimates of Median Monthly Mixed-Layer Depth for Harvard Forest

Month	n	Boundary Layer Depth, m	HF Air Temperature, °C	n_T
Jan.	237	674	-3	120
Feb.	270	688	-2	178
March	253	1031	2	146
April	273	1147	10	145
May	285	1673	15	166
June	299	1744	19	185
July	306	1748	20	209
Aug.	309	1751	21	157
Sept.	335	1178	17	247
Oct.	325	1119	11	232
Nov.	309	703	5	220
Dec.	322	681	0	211

The top of the mixed layer was determined from gridded NGM data for each back trajectory calculated in this study.

Note: n is the number of back trajectories calculated during the month; HF air temperature is the mean monthly ambient air temperature corresponding to each trajectory time as measured on the Harvard Forest tower; n_T is the number of temperature measurements used (n_T is consistently lower than n because of missing data).

Figure 1 illustrates the median mixed-layer height by season and time of day. From this it is apparent that the mixed layer is significantly more shallow in the morning and is deepest during the afternoon. Again, this is consistent with the earlier results of *Holzworth* [1967]; however, the average afternoon mixed-layer depths in this study are deeper by 200-400 m. Given that these mixed-layer depths are based on the temperature structure from the NGM model, which has only 10 vertical levels between the surface and 400 mbar, this overestimate may be real. If no stable layers (regions where the potential temperature exceeded 1° C km^{-1}) were detected in the model profile, then the mixed-layer depth defaulted to the top sigma level. These cases will contribute to this overestimate. In spite of the shortcomings inherent in using this regional-scale model with its limited resolution, we have made this effort to characterize changes in mixed-layer depth. This variability can have multiple effects on chemical concentrations. For example, diurnal variation in mixed-layer depth contributes to diel concentration cycles. For local or surface source pollutants (like anthropogenic hydrocarbons and CO), the concentrations can build up over night, so that maximum concentrations will be observed in the morning, and as the mixed layer deepens, concentrations will be diluted [*Munger et al.*, 1996]. However, for a depositing species like O_3, concentrations may be depleted in a shallow mixed layer. Furthermore, if the transport of photochemically aged air is making a contribution to the site, concentrations of O_3 are likely to increase as the mixed layer deepens and air masses that have been isolated from the surface are mixed downward. This entrainment mechanism can also contribute to increased ozone from natural sources, particularly in late winter and spring when stratospheric intrusions into subsiding air masses are expected to contribute to enhanced ozone in the free troposphere [*Moody et al.*, 1995].

Three different averaging periods were established to describe the chemical data corresponding to trajectories. Each 0700 trajectory was matched with chemical data representing the 3-hour average from 0600-0900 LST on that day. The 1100 trajectory was matched with chemical data representing the 3-hour average from 1000-1300, and each 1500 trajectory was matched with chemical data representing the 3-hour average from 1400-1700 on that day. The 3-hour averages were calculated using available data, so if 2 of the 3 hours were missing, the 1-hour value present represents the mean for that averaging period. This helped to reduce the impact of missing chemical data.

2.2. Back Trajectory Pattern Analysis

To identify days characterized by similar regional-scale transport, we analyzed the trajectory data using a pattern recognition routine. The University of Virginia (UVA) Patterns in Atmospheric Transport History (PATH) model was developed to accomplish this task. The result of the PATH analysis is a number of sets of back trajectories, with each set represented by trajectories which describe similar 3-D transport to the receptor. Similarity is quantified relative to the overall amount of variability present in the modeled

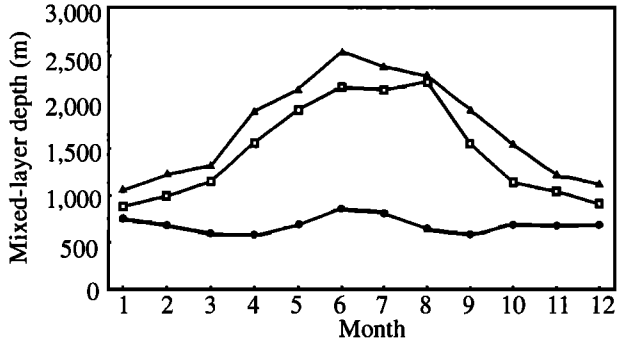

Figure 1. Seasonal and temporal variations by time of day (solid circle, 0700 EST; open square, 1100 EST; solid triangle, 1500 EST) in the monthly average mixed-layer depth at Harvard Forest as calculated by the National Meteorological Center Nested Grid Model.

trajectories. The trajectories are quantified using endpoints defined in latitude, longitude, and pressure coordinates. These variables are standardized to have a mean of 0 and a standard deviation of 1. The Euclidean distance of each trajectory to every other trajectory in the entire data set is calculated as follows:

$$D_{ij} = \sqrt{\sum_{k=1}^{n} (z\mathrm{lat}_{ik} - z\mathrm{lat}_{jk})^2 + (z\mathrm{lon}_{ik} - z\mathrm{lon}_{jk})^2 + (z\mathrm{p}_{ik} - z\mathrm{p}_{jk})^2}$$

This represents the three-dimensional distance between two trajectories i and j, where k is the number of back trajectory endpoints used to characterize the transport. For the work presented here, k=24; and, since these are 2-hour model time steps, the distance describes the relative similarity of trajectories going back 48 hours. Trajectories were calculated 72 hours back; however, more than 15% of these left the model domain or encountered missing meteorological data before extending 3 full days back. Therefore, 48 hours was determined to be sufficient to identify regional-scale transport patterns and retain over 85% of the trajectories as complete.

To group the trajectories, we chose a radius of proximity and, using each trajectory recursively as a center, located all the trajectories determined to be within the radius of proximity to that center. In this way, we defined a neighborhood of proximate trajectories for each individual trajectory. Initially, these groups were not exclusive. We defined the core of the first feature, or path, by selecting the individual trajectory with the largest neighborhood, the largest number of trajectories within the radius of proximity. These were grouped together, and these trajectories were removed from the analysis. The neighborhoods for each trajectory were then recalculated; and, again, the trajectory with the largest number of neighbors within the radius of proximity was selected and its members were removed from the analysis. The designation of pattern centers continued until there was no longer a center which had at least 2.5% of the original number of trajectories within a radius of proximity (this excluded the formation of small, statistically insignificant, flow features); thus the procedure continued until no valid neighborhoods remained. At this point, all of the ungrouped trajectories were reanalyzed to assign them to the nearest flow feature, by calculating their distance from the central trajectory of each feature. If a trajectory was more than twice the radius of proximity from every feature center, then it was classified as an outlier. This effectively produced a two-tiered result: a very distinctly defined set of transport pattern centers, or flow features, and a more diffuse set of classified trajectories, or general PATHs, which included all but extreme outlier trajectories.

Canned cluster analysis routines have been applied to back trajectory data in several studies presented in the literature [*Moody et al.*, 1995; *Sirois and Bottenheim*, 1995; *Moy et al.*, 1994; *Dorling et al.*, 1992; *Harris and Kahl*, 1990; *Moody and Samson*, 1989; *Moody and Galloway*, 1988]; however, the PATH algorithm has several distinct advantages. While the determination of a radius of proximity is an adjustable quantity, this is in fact desirable, to be able to quantify the definition of similarity among the trajectories. For trajectories from a given location, this designation initially determined by iteration, can be set as a constant, which allows different sets of trajectories to be analyzed for a site using the same criteria. Finally, in addition to controlling the "clustering" process, this model is computationally more efficient, and we can effectively analyze a very large multiyear set of trajectories. Although in past work we have determined separate flow patterns for different seasons, it then becomes difficult to compare one set of seasonally defined flow patterns to another. For this paper, one set of flow patterns was defined for the entire data set, using a proximity radius of 15.7.

2.3. Chemical Measurements

The Harvard Forest LTER site is in Petersham, Massachusetts, located 100 km west of Boston and 100 km north of Hartford, Connecticut. Chemical measurements at Harvard Forest are made on a 30-m tower which extends above the forest canopy. The surrounding region is sufficiently uniform for eddy-flux measurements [*Moore et al.*, 1996] so that in addition to trace gas concentrations, surface exchange fluxes, including energy and momentum fluxes, are continuously measured. A thorough discussion of the analytical measurement methods, as well as data precision and accuracy, is presented by *Munger et al.* [1996].

3. Results

3.1. Designation of PATH

Plate 1 shows the trajectory PATHs derived from the data from January 1, 1990, through December 31, 1993. The probability mapping illustrates the likelihood of trajectories having passed over a location, with warmer colors (e.g., pink) representing higher probability. These fields are based on a method of representing each back trajectory as a two-dimensional probability field [*Samson and Moody*, 1981] and summing the probability fields of all trajectories making up a PATH. The probability field is normalized relative to the maximum probability associated with a given grid cell, with the probabilities calculated on a grid approximately 80x80 km square at the latitude of Harvard Forest. The contour intervals designate grid cells where the probability of a trajectory passing over that cell was 10% of the maximum probability, 20% of the maximum probability, 30% of the maximum probability, etc. up to the grid cell with the highest

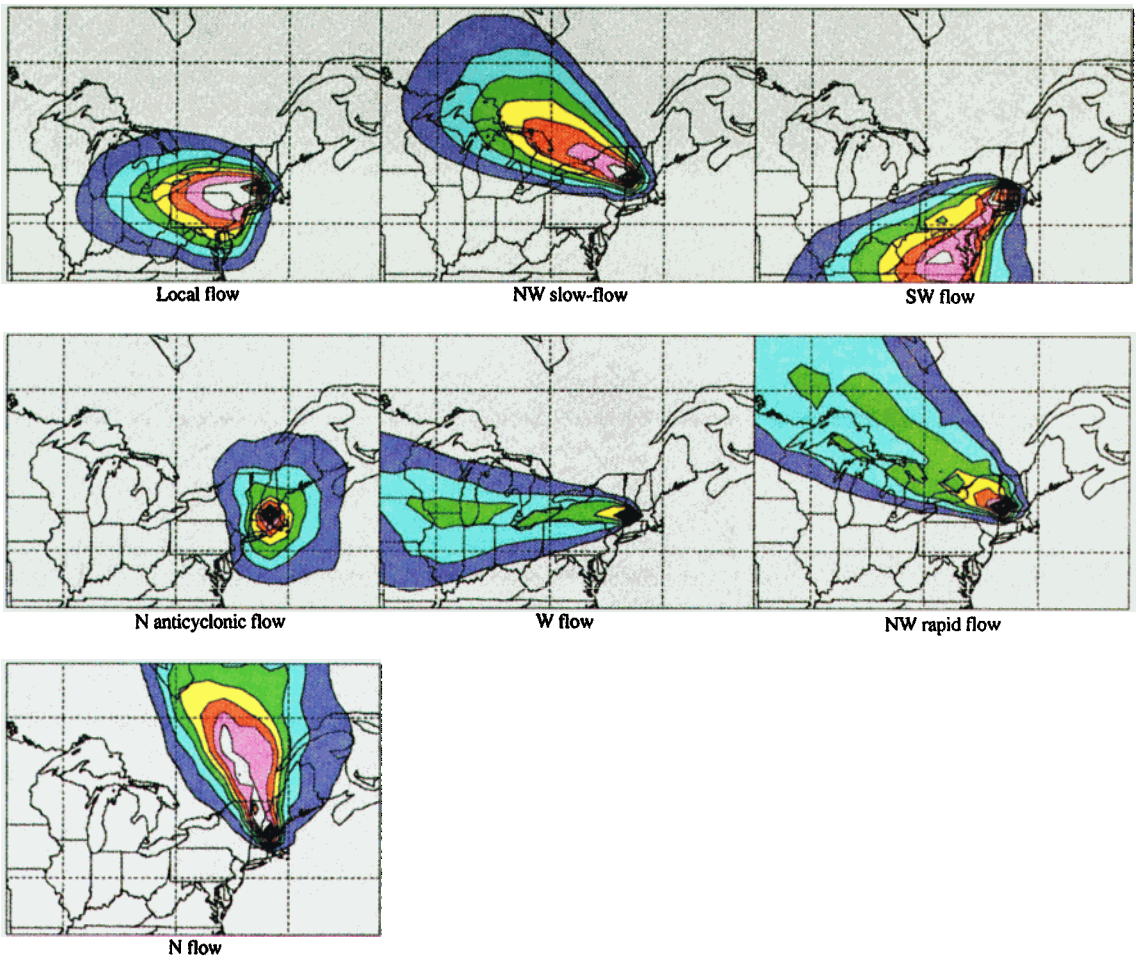

Plate 1. PATH model results depicting seven different flow patterns. Relative probability is contoured; it represents the likelihood of trajectories having crossed the underlying regions. Ten probability intervals are contoured; warmer colors show higher probability.

probability (which is always the receptor cell). In this way, we can establish a pattern that illustrates the upwind regions the trajectories were most likely to have passed over during the previous 48 hours.

Each flow pattern has been assigned a descriptive name which gives an indication of the transport represented by these back trajectories. The names of these patterns and their frequency of occurrence are shown in Table 2. We can compare the relative frequency of occurrence of each PATH by season, as shown in Figure 2. From this, it is apparent that there is a greater occurrence of relatively low-speed transport "local" flow during the warm half of the year (22% versus 17%), as well as a higher frequency of warm season high-pressure days illustrated by anticyclonic transport patterns (15% versus 10%). By contrast, the cool months show a higher frequency of transport from a westerly or northwesterly direction (45% versus 36%).

3.2. Seasonality by PATH

In Figure 3, we have plotted median chemical mixing ratios of O_3 and CO by month, using all the available data (i.e., all the 3-hour averages for the trajectory times of 0700, 1100, and 1500). It is apparent that there is a strong seasonality in the chemical data. This is a function of both chemical and physical conditions, such as seasonally variable chemical transformation rates, variable emissions or source strength, and seasonal differences in mixed-layer depth. A combination of these factors results in the observation that higher concentrations of primary pollutants like CO (and many hydrocarbons) occur in the morning hours during cold months when low boundary layer mixing depths minimize dilution (Figure 3). Ozone, which has both anthropogenic photochemical sources and natural sources as well as significant surface sinks present in the summer forest canopy, shows a very typical eastern North American seasonality, with a relatively weak but broad early summer maximum with a May-June peak analogous to the seasonal pattern observed at Whiteface Mountain, another rural NE location which is at a much higher elevation [*Chai and Mohnen*, 1998].

Now that we have characterized the general seasonal pattern of all the data, we can assess the differences in monthly medians as a function of trajectory PATH. Monthly median mixing ratios of CO, O_3, and ethane have been plotted for five of the seven flow PATHs. In Figure 4a, CO, an example of a combustion-derived gas, follows a similar seasonal pattern for all paths, but the magnitude of the signal is a function of the air mass origin. Trajectories from the N and NW-fast effectively describe a CO background (lowest

Table 2. PATH Designation and Frequency of Occurrence Along With Average Mixed-Layer Depths Based on All Daytime Trajectories (0700, 1100, and 1500 LST)

Flow PATH	n	Annual Frequency of Occurrence, %	Average Mixed-Layer Depth,* m	12-hr Subsidence Rate,† mbar
Local: light winds, moderate mixed layer	708	20	1210	-2 (25)
NW-slow: moderate winds, moderate mixed layer, moderate subsidence	618	18	1245	-29 (23)
SW: warm, moist, moderate mixed layer, rising motion	512	15	1210	23 (30)
Anticyclonic: trajectories loop around from the N to arrive from the S, SW; shallow mixed layer, cool but moist	462	13	875	6 (32)
West: warm, dry, deep mixed layer, strong winds, subsidence	415	12	1780	-17 (31)
NW-fast: strong winds, cool, dry, deep mixed layer, strong subsidence	428	12	1560	-64 (29)
N: moderate winds, moderate mixed layer, cool, dry, moderate subsidence	380	11	1220	-37 (32)

*Calculated for the Harvard Forest grid cell in National Meteorological Center Nested Grid Model.
†Pressure difference between 0 and 12 hours upwind; negative values indicate subsidence is occurring as the trajectory approaches the Harvard Forest site.

mixing ratios, lowest variance) that ranges from 110 ppb during the summer to ~190 ppb during the winter. By contrast, trajectories arriving from the SW deliver enhanced mixing ratios of CO in all months of the year, ranging from 160 to 220 ppb during the summer up to ~300 ppb during winter months. Both the SW and Local trajectory transport patterns are clearly impacted by anthropogenic source regions, leading to a strong pollution signal. As we will show, NO_x, NO_y, and hydrocarbons all exhibit elevated concentrations under these flow patterns as well. Anticyclonic and NW-slow transport were not plotted to maintain clarity in the figure; however, they fall between the extremes presented here, with NW-slow flow looking like the background and with anticyclonic trajectories showing some influence of anthropogenic sources. This is consistent with the observation that many of the trajectories in this path represent flow around a cell of high pressure situated over the northeast. They have an origin to the north and west of the site, but they curve anticyclonically to arrive from the east or southeast, off the ocean, but potentially being influenced by recent emissions as they cross heavily populated regions of the eastern urban corridor upwind of Harvard Forest.

Variations in O_3 show a very different seasonal pattern (Figure 4b). Ozone is both a secondary pollutant, the result of photochemical production in polluted air masses, and it has a primary natural source, as O_3 transferred from the stratosphere during dynamic events in the upper troposphere. Trajectories from the N exhibit a seasonal signal different from the other flow paths which looks like the signal of natural background O_3. There is very good correspondence between the spring peak in N flow at this site and other relatively remote northern hemisphere locations like polar continental air observed at Kejimkujik, Nova Scotia [*Sirois and Bottenheim*, 1995], and the total set of observations from Reykjavik, Iceland, and Mace Head, Ireland (with spring peaks, ~42 ppb [*Oltmans and Levy*, 1994]). Reykjavik observes lower mixing ratios in July (~ 20 ppb) relative to Harvard Forest N-flow, but this is consistent with a higher contribution of low-level marine transport, which is depleted in ozone, reaching that site during the summer. Mace Head mixing ratios of O_3 in the early autumn (~ 35 ppb) are higher than observations for Harvard Forest during autumn, but Mace Head is periodically influenced by anthropogenic contributions from European sources and may not represent background conditions. The summer peak is superimposed on this background signal and should represent ozone production. *Hirsch et al.* [1996] describe some of this summer seasonality

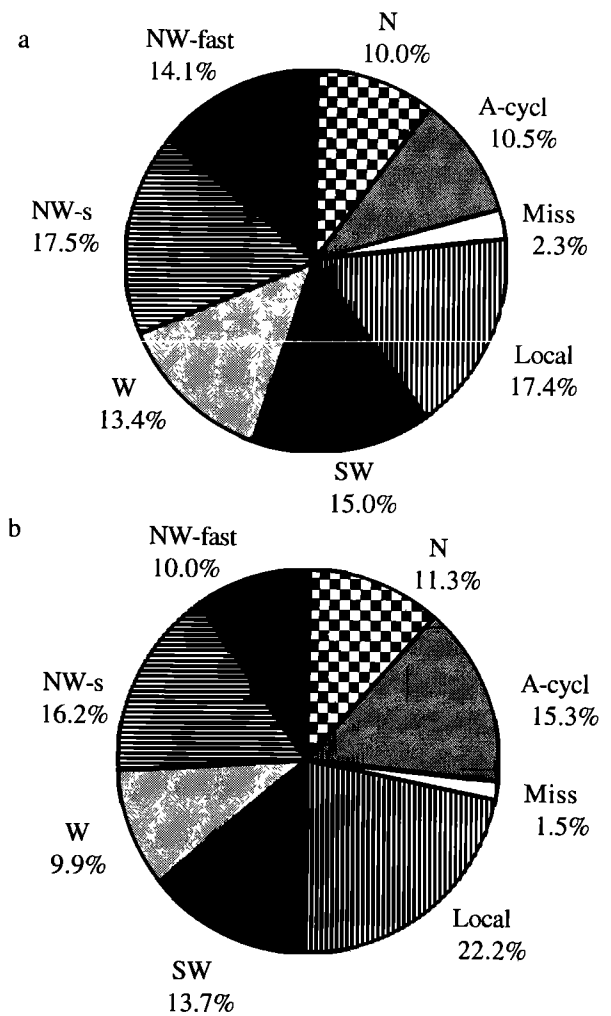

Figure 2. Relative frequency of occurrence of transport patterns at Harvard Forest during (a) the cold season (October-March) and (b) the warm season (April-September).

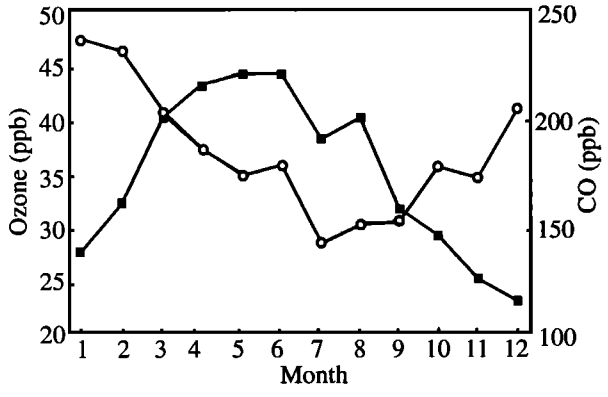

Figure 3. Monthly median mixing ratios showing seasonal signals for O_3 (solid squares) and CO (open circles).

in terms of ozone production efficiency changing in response to the availability of isoprene. This is discussed in section 4.1. Figure 4b shows that the greatest enhancement over background ozone is associated with the westerly and local flow PATHs.

In Figure 4c, we illustrate the seasonal variation in ethane by flow path. Again, the northerly transport path delivers the lowest concentrations in every month and looks very similar to the 10th percentile presented by *Goldstein et al.* [1995b]. In that paper, the seasonality in background ethane was shown to be driven mainly by chemical transformation rates, and ethane was determined to be a good tracer for analysis of hemispheric mean OH. We see relatively similar seasonal amplitude across different flow patterns; however, like CO, the magnitude of ethane is dependent on transport, with flow from more polluted geographical regions (SW, W, Local PATHs) contributing to enhanced concentrations throughout the year.

For the Harvard Forest transport patterns associated with high concentration of both short and long-lived pollutants (e.g., CO, NO_x, and ethane in Local and SW flow), we see a distinct minimum in O_3 under these conditions in winter. However, during the summer, under these polluted flow patterns, some of the photochemical production potential of these emissions are realized, and concentrations are enhanced of the order of 10-15 ppb over background (if we consider background to be represented by the northerly path). However, the highest ozone mixing ratios in the summer are associated with transport from the west. These trajectories are correlated with sunny skies, deep mixed layers, above average temperatures, enhanced isoprene concentrations, and relatively low water vapor conditions, and the median O_3 is 20 ppb above the background. We will show that these air parcels may be more photochemically productive, and, based on transport PATH, they suggest a contribution from Midwestern source regions to regional-scale O_3 events over the northeastern United States. This ozone contribution is greater than the oxidant levels associated with flow from the SW which encompasses major eastern urban centers.

3.3. Summary of PATH Physical and Chemical Characteristics

In order to summarize the chemical differences in air mass composition based on differences in atmospheric transport history, it is important to take into account the significant

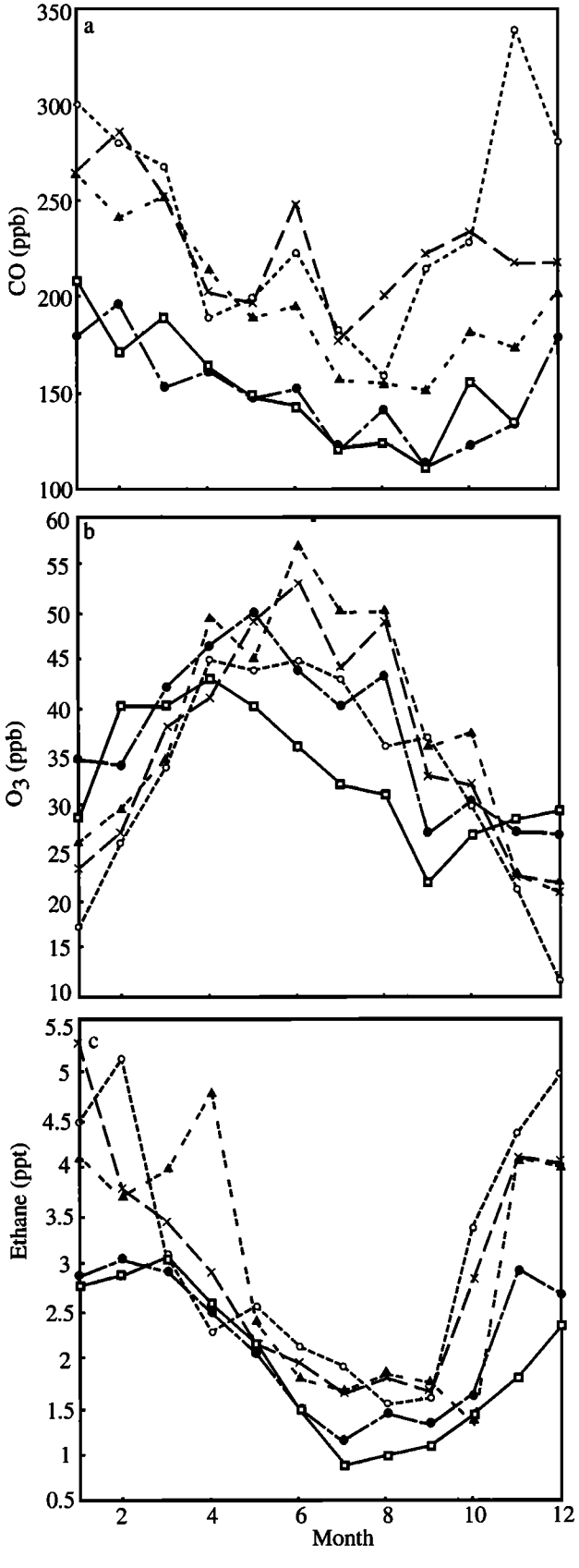

Figure 4. Monthly median mixing ratios showing seasonal signals for (a) CO, (b) O_3, and (c) ethane under different PATHs (x, Local; open circle, SW; closed triangle, W; closed circle, NW-fast; and open square, N).

monthly variation illustrated in the last section. Therefore the data were grouped into quarterly periods, and for the winter (December-February) and summer quarters (June-August), we have plotted the following for each PATH: the deviation of the mean of each species from the mean for the quarter (Figures 5-7). This approach gives a quick look at the PATHs with relative enhancements or relative depletions of each chemical species. To aid the interpretation of these figures, the quarterly means are included in Table 3. In addition to chemical parameters, temperature, water vapor mixing ratio, mixed-layer depth, and photosynthetically active radiation have been plotted the same way; they are shown in Figures 7a and 7b. As shown in the monthly plots, the spring and fall quarters were periods of transition with less chemical difference based on trajectory PATH, and therefore they have been omitted from this analysis.

Figures 5a and 5b summarize the daytime O_3, CO, NO_x, NO_y, and acetylene (using data from all three averaging periods) for summer and winter (as defined above), respectively. A larger set of hydrocarbons is presented in Figures 6a and 6b, it shows that ethane, ethene, butane, and acetylene behave similarly between flow PATHs. From these figures, the inverse relationship of O_3 and CO during the winter (as discussed by *Parrish et al.* [1998] for sites in the North Atlantic region) is apparent, with O_3 mixing ratios 20-40% greater than the winter mean in the northerly flow paths, when CO was 20% below the winter average. In contrast, O_3 mixing ratios were below the winter mean in Local and SW patterns where CO was 40% above the winter average (Figure 5a). It is readily observed that during the summer, all species exhibit lower mixing ratios under flow with a northerly component (Figure 5b and 6b). Ozone, which is typically a secondary pollutant during the summer, is highest in W flow. However, the relatively slow moving transport pattern characterized as local flow was generally most polluted, with

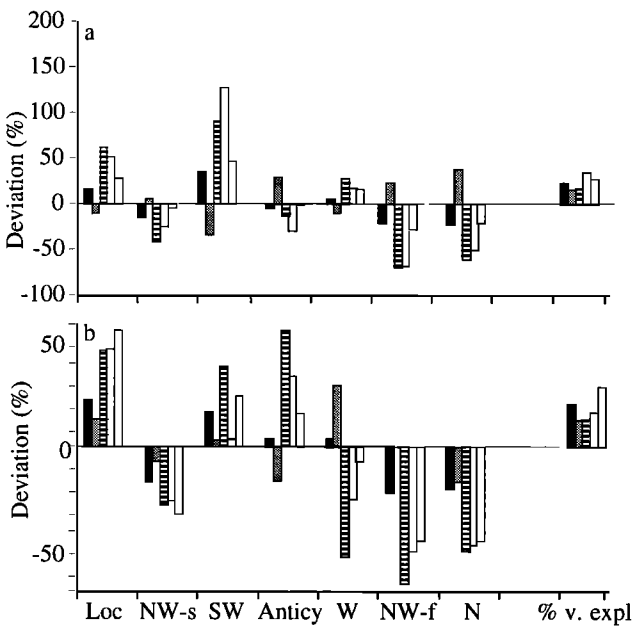

Figure 5. Deviations of mean mixing ratios within each PATH from the seasonal mean mixing ratio of CO (solid column), O_3 (dark gray column), acetylene (striped column), NO_y (light gray column), and NO_x (open column) for (a) winter (December-February) and (b) summer (June-August).

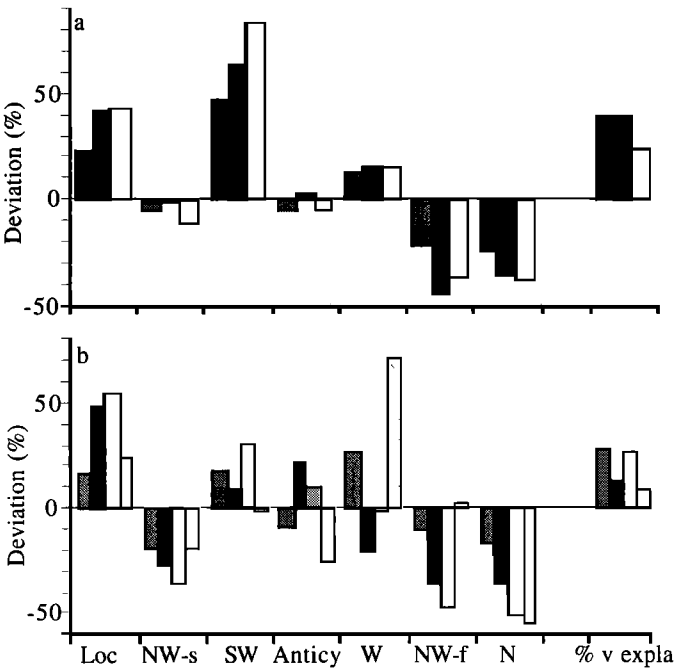

Figure 6. Deviations of mean mixing ratios within each PATH from the seasonal mean mixing ratio of ethane (dark gray column), ethene (solid column), butane (open column), and isoprene (light gray column) for (a) winter (December-February) and (b) summer (June-August). Isoprene was undetectable during winter.

enhancements of all species. In SW flow, we also found enhancements of CO, NO_x, and acetylene, but on the average, these air masses were associated with relatively low O_3 and NO_y, either as a result of less chemically aged air reaching the site under these flow conditions, or as a result of cloud cover and precipitation suppressing O_3 and removing NO_y, respectively. Looking at the physical character of air parcels, the air temperature is above average in flow from the SW along with high water vapor mixing ratios (Figure 7b). We also see a significant variation in the amount of photosynthetically active radiation (PAR) used here as a measure of cloudiness. We see that the clearest days occur with flow from the W and NW, under deep mixed layers, while the cloudiest days are associated with flow from the SW. These results contribute to a synoptic interpretation, which for the SW path suggests transport ahead of a warm front, or in the warm sector of a low-pressure center ahead of an advancing cold front. This is consistent with the delivery of warm moist air, and higher concentrations of pollutants from the significant source regions upwind in this direction, the East Coast urban corridor. In addition to fresh emissions, the increased cloudiness may also contribute to lower O_3 in this PATH. At the opposite extreme, the NW-fast PATH is consistent with transport behind a cold front, with deep mixed layers, cooler temperatures, and significant sunshine delivering clean air. During the cold season, we found similar variations in composition, with higher mixing ratios of CO, NO_x, NO_y, and ethane, in flow from the SW under conditions of higher temperatures and water vapor mixing ratios and more cloud cover. The lowest water vapor occurred with W, N, and NW flow, under relatively cloud-free skies in association with relatively low pollutant levels and slightly enhanced ozone (Figure 7a).

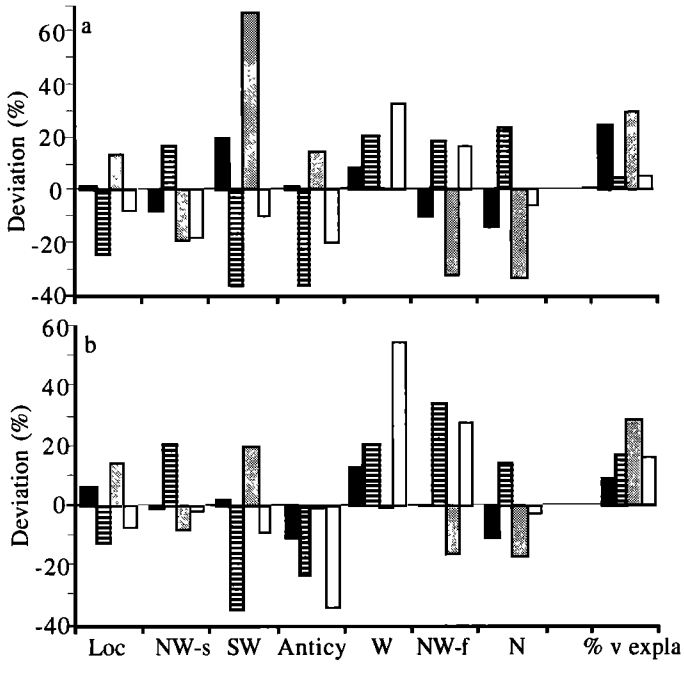

Figure 7. Deviations of mean mixing ratios within each PATH from seasonal mean air temperature (solid column), photosynthetically active radiation (striped column), water-vapor mixing ratio (shaded column), and mixed-layer depth (open column) for (a) winter (December-February) and (b) summer (June-August).

Although we can readily develop a broad synoptic distinction between these flow paths, the standard deviations around the chemical means typically overlap indicating a substantial amount of residual variance within each flow PATH. One factor that may account for some of this variation within transport patterns is the time of observation. These figures represent a mixture of all the analyzed trajectories and their associated chemistry from 0700, 1100, and 1500. In the next section, we look at chemical differences by PATH separately for each of these trajectory times.

3.4. Analysis of Variance

In this section, we analyze the variance in chemical and physical observations which can be explained by differences in atmospheric transport history. Initially, nonparametric tests (conservative statistics for assessing significant differences in the central tendency of distributions which show deviations from normality) were used to identify differences in chemical distributions between flow paths. If statistically significant differences were detected, a standard parametric analysis of variance was then applied to estimate the amount of variance explained by flow path. In addition to monthly variation, we know that there is diurnal variation in these reactive tracers, so we have taken into account both the time of day and time of year represented by each 3-hour average observation. The quarters were defined as December through February, March through May, June through August, and September through November. The averaging periods represent 3-hour averages surrounding the hour of the trajectory, as described in the methods section.

Table 4 summarizes the analysis of variance results comparing the chemical distributions between flow paths. It shows a breakdown of the amount of variance in CO concentration (for example) which is explained by different atmospheric transport history for each quarter and each averaging period. Between ~15 and 30% of the variability in CO mixing ratios may be explained by differences in air mass origin. This leaves a relatively large amount of the variance in CO within transport patterns. For O_3, we find somewhat less of the variability explained by PATH. We can also see from this table that, during the spring and the fall, there is no significant variability in O_3. In contrast, relatively large amounts of variance are consistently explained for the hydrocarbons in all four quarters of the year. However, even for ethane where 20-50% of the variance may be a function of transport history, there is a residual, or unexplained variance. The lower part of this table illustrates the significant variation in meteorological variables like water vapor mixing ratio, temperature, and photosynthetically active radiation, representative of cloud cover among flow PATHs.

In summary, we find that trajectory-defined regional-scale transport PATH can explain a statistically significant amount

Table 3. Seasonal Means and Standard Deviations of the Variables Presented in Figures 5 through 7

Observation	Winter		Summer	
	Mean	s.d.	Mean	s.d.
Temperature	-1.6°C	6.5 °C	20.3 °C	5.3°C
PAR	268	297	873	485
H_2O_v	2.79 gm kg^{-1}	1.6 gm kg^{-1}	8.45 gm kg^{-1}	2.01 gm kg^{-1}
Elevation	918 m	509 m	1743 m	1069 m
O_3	29.6 ppb	15.5 ppb	44.3 ppb	17.2 ppb
CO	247 ppb	93 ppb	172 ppb	64 ppb
NO_x	8.8 ppb	11.8 ppb	1.8 ppb	2.3 ppb
NO_y	11.4 ppb	12.1 ppb	5.0 ppb	4.4 ppb
Acetylene	1.23 pptv	0.53 pptv	0.44 pptv	0.29 pptv
Ethane	3.54 pptv	1.26 pptv	1.53 pptv	0.54 pptv
Ethene	1.02 pptv	0.74 pptv	0.51 pptv	0.46 pptv
Butane	1.03 pptv	0.63 pptv	0.29 pptv	0.223 pptv
Isoprene	NA*	NA*	3.11 pptv†	2.49 pptv

Winter is defined as December-February; summer is June-August.

*Not applicable; isoprene is below detection limit in winter (<10 pptv).

†Isoprene recovery in the analytical system was less than 100% before 1995. The relative difference between PATHs should be consistent, but the absolute values are low. To better estimate the relative magnitude of isoprene by PATH, the mean and standard deviation (s.d.) for 1995 summer daytime data are presented here (A. H. Goldstein, personal communication, 1997).

Table 4. Estimates of Variance Explained by Comparing Chemical and Physical Constituent Distributions Between Flow PATHs for Specified Periods Defined by Quarter and the Time of Day

	0600-0800				1000-1200				1400-1600			
	Q1	Q2	Q3	Q4	Q1	Q2	Q3	Q4	Q1	Q2	Q3	Q4
CO	20	15	34	12	29	--	18	25	25	18	21	13
O_3	15	NA*	28	--	19	--	13	--	22	--	10	--
NO_x	17	8	13	15	17	--	11	17	25	--	--	16
NO_y	32	13	21	20	31	9	17	22	48	9	17	16
Ethane	34	10	43	32	36	33	33	17	56	23	24	19
Acetylene	39	16	34	25	33	30	28	23	30	38	28	28
Isoprene	--	--	10	--	--	--	24	--	--	--	--	--
Ethene	41	21	26	17	19	34	0	18	29	32	22	22
H_2O_v†	33	34	30	21	36	41	31	18	30	31	29	19
Temperature‡	28	18	10	24	25	18	10	16	28	--	--	12
PAR§	10	5.6	27	9	20	19	15	17	16	16	20	7
Wind speed	8	23	10	4.4	9	17	10	--	9	10	--	--

Note: Quarter 1(Q1) is December-February; Q2 is March-May; Q3 is June-August; and Q4 is September-November.
*No significant difference in composition of this constituent was detected between flow PATHs for this quarter and averaging period.
†Water vapor mixing ratio calculated from the T, RH, and pressure at the site.
‡Ambient temperature measured on the Harvard Forest tower.
§Photosynthetically active radiation.

of the variation in chemical species with mainly anthropogenic sources and with long lifetimes; it can also account for different physical air mass characteristics like water vapor content. However, for a reactive species like O_3, which has both photochemical and natural sources, and variable loss mechanisms, this general approach to assess variability in mixing ratios is less effective.

4. Discussion

There are several factors which may introduce variability into the chemical composition for periods characterized to have similar regional-scale transport history. One is mixed-layer depth, or the amount of vertical mixing. *Munger et al.* [1996] has hypothesized that the trapping of emissions near the surface in shallow mixed layers contributes to diel chemical cycles. In this paper, we used the NGM model mixed-layer depth to make some comparisons. For example, we compared CO versus mixed-layer depth under SW transport for the winter quarter only (December-February). We found 83% of the high CO mixing ratios (greater than 250 ppb) were associated with mixed layers less than 1000 m deep. By contrast, only 37% of CO mixing ratios less than 250 ppb in this PATH had mixed-layer depths of 1000 m or less. A similar analysis of the Local PATH in the warm season (which also had high median CO mixing ratios) found

Table 5. Ozone Production Efficiency, Regression Results of O_3 Versus NO_x Oxidation Products, Comparison of Harvard Forest With the Literature, and Variations of Ozone Production Efficiency and Average Photochemical Age by PATH

Location	Regression	Variance Explained	Reference	
Eastern United States	$O_3 = 8.5\ (NO_y\text{-}NO_x) + 35$	$r^2 = 0.99$	Trainer et al. [1993]	
Rural Georgia	$O_3 = 11.4\ (NO_y\text{-}NO_x) + 27$	$r^2 = 0.78$	Kleinman et al. [1994]	
Giles County, Tennessee	$O_3 = 12.3\ (NO_y\text{-}NO_x) + 41$	$r^2 = 0.59$	Olszyna et al. [1994]	
Harvard Forest				
August	$O_3 = 8.6\ (NO_y\text{-}NO_x) + 35$	$r^2 = 0.93$	Hirsch et al. [1996]	
May	$O_3 = 3.9\ (NO_y\text{-}NO_x) + 33$	$r^2 = 0.78$	Hirsch et al. [1996]	
Harvard Forest (all 1500 data)	$O_3 = 7.1\ (NO_y\text{-}NO_x) + 28$	$r^2 = 0.48$	this paper	
PATH	**Regression**	**Variance Explained**	**$\Delta O_3/\Delta CO$**	**$(1\text{-}NO_y/NO_x)$†**
Local	$O_3 = 7.7\ (NO_y\text{-}NO_x) + 19$	$r^2 = 0.55$	0.43	0.67
NW-s	$O_3 = 5.5\ (NO_y\text{-}NO_x) + 34$	$r^2 = 0.24$	0.42	0.74
SW	$O_3 = 5.7\ (NO_y\text{-}NO_x) + 29$	$r^2 = 0.70$	0.21	0.56
Anticyclonic	$O_3 = 11.1\ (NO_y\text{-}NO_x) + 14$	$r^2 = 0.58$	0.28	0.63
W	$O_3 = 8.7\ (NO_y\text{-}NO_x) + 32$	$r^2 = 0.73$	0.42	0.74
NW-f	$O_3 = 6.7\ (NO_y\text{-}NO_x) + 32$	$r^2 = 0.37$	0.27	0.70
N	$O_3 = 7.4\ (NO_y\text{-}NO_x) + 26$	$r^2 = 0.49$	0.25	0.66

*O_3 versus CO excluding fresh pollution ($NO_y\text{-}NO_x < 0.3$).
†Average photochemical age.

that 59% of the CO mixing ratios greater than 250 ppb occurred within shallow mixed layers of 1000 m or less although only 31% of the CO mixing ratios less than 250 ppb occurred with these shallow mixed depths. In addition, we know that even under the same transport PATH, some trajectories may have passed more directly over specific source regions. It is also apparent that if the air parcel elevation as some time upwind is above the local mixed-layer depth for that source region, it is unlikely that the air parcel will be influenced by surface emissions from that location.

In order to more specifically address the residual variation within transport PATHs, we will need to look at extreme events within a given transport pattern for a specific averaging time, and quarter, and more carefully assess the meteorological conditions associated with each of these chemically anomalous events. These case studies will be presented in a separate paper.

4.1. O_3 Versus Other Pollutants

The statistically significant differences in composition between flow paths presented in section 3 are enough to provide a general picture of the ways in which regional-scale transport influences chemistry. However, we would also like to discern differences in chemical ratios which might help explain different atmospheric processing based on atmospheric transport history.

In an effort to assess differences in O_3 sources, and air mass photochemical age, we have focused on the late morning, and afternoon period (1000-1300 and 1400-1700), using only data from the summer months (June-August). We have estimated the NO_x oxidation products as NO_z=NO_y-NO_x, and we have analyzed the O_3 mixing ratio versus this variable and versus CO. *Trainer et al.* [1993] presented results for six sites in the eastern United States that show O_3 is highly correlated with the quantity NO_z. Similar slopes of O_3 to NO_2 were reported for these locations. *Olszyna et al.* [1993] and *Kleinman et al.* [1994] applied the same analysis to data from rural Tennessee and Georgia, respectively, and found comparable slopes. These analyses are based on the assumption that there is a relationship between the number of NO_x molecules oxidized and the number of O_3 molecules formed, and the strength of the relationship provides an upper bound on the photochemical production efficiency of an air mass. They point out that to have a high correlation the O_3 production must have occurred in the relatively recent past or else NO_y, which is removed during transport by wet and dry deposition processes, may not be a reliable indicator. Modeling studies have indicated a nonlinearity, with O_3 production efficiency decreasing with increasing NO_x levels [*Lin et al.*, 1988]. *McKeen et al.* [1991] demonstrated that higher hydrocarbon to NO_x ratios will enhance the amount of O_3 formed per NO_x oxidation.

The work of *Jacob et al.* [1995] in Shenandoah Park, Virginia, provides observational evidence that the O_3 production efficiency over the eastern United States may be a function of the UV radiation and humidity which control the level of odd-hydrogen radicals. They show that the O_3 production efficiency declines with a decrease in odd-H production. This is consistent with the theoretical expectation of a seasonal transition from NO_x-limited to hydrocarbon-limited O_3 production as odd-H drops to less than 2 times the NO_x emission rate, and NO_x oxidation becomes the primary sink for odd-H radicals [*Sillman et al.*, 1990]. Declining biogenic hydrocarbon emissions (e.g., isoprene) which result from leaf senescence may accentuate this transition since oxidation of isoprene is a significant source of odd-H. *Hirsch et al.* [1996] extend this relationship to Harvard Forest, illustrating that a seasonal pattern in O_3 production efficiency may reflect changes in the availability of isoprene.

To the extent that O_3 production efficiency is a function of NO_x and hydrocarbon emissions, as well as UV flux, it is reasonable to look for significant variation in O_3 versus NO_z regression slopes as a function of PATH. In this analysis, we have used all the 3-hour average O_3, NO_x, and NO_y corresponding to clustered trajectories. We excluded two cases where NO_y-NO_x was greater than 12 ppb, indicative of fresh emissions. The overall data (June-August) from Harvard Forest appears to have a comparable slope relative to these other studies (Table 5), with a value of 7.1 and a background O_3 concentration of 28 ppb. Similarly, a regression between O_3 and CO yields a slope of 0.33, close to the 0.30 value typical of eastern North American boundary layer air [*Chin et al.*, 1994; *Parrish et al.*, 1993]. However, these slopes will tend to be driven by distribution end-members representing the most clean and most polluted conditions, respectively. In fact, when we look at the relationship between O_3 and estimated oxidation products by PATH, there are significant differences in chemical relationships, and it is useful to consider these.

The transport pattern of SW flow has the lowest slope with an r^2 that explains at least 50% of the variance. The regression for this PATH indicates 5.7 ppb of O_3 for each ppb of NO_z. This flow pattern also has the lowest average photochemical age (0.56), the highest CO concentrations and the lowest average O_3 versus CO slope of 0.21. All these are indicative of the strong influence of fresh emissions under this flow pattern. This chemical signal is consistent with the air mass history suggested by these events which illustrate a significant contribution from urban industrial sources to the SW. In addition, these events are relatively cloudy, with the lowest average PAR measured at Harvard Forest in this flow pattern. In contrast, the W PATH had a greater slope of 8.7 ppb per ppb of NO_z. This transport pattern delivered air with a higher average photochemical age (0.74) and a greater O_3 versus CO slope of 0.42. It was already shown that these events had the highest average temperatures and isoprene levels, under generally clear conditions, with deeper mixed layers and above average wind speeds measured at the site. The largest slope (11.1 ppb) occurred under the anticyclonic PATH. However, the ratio is likely driven by relatively low NO_z which along with the transport pattern may indicate air that has had NO_y removed. This would also account for the apparently low average photochemical age. Local PATH chemistry was similar to the W PATH with comparable O_3 versus CO slopes, and high isoprene concentrations; however, the NO_x concentrations were much higher under the low wind speed local PATH conditions. Higher NO_x results in a lower average photochemical age and a lower slope.

The correlations between O_3 and NO_z for NW-slow and NW-fast and N flow are weaker than for other transport PATHs with less than 50% of the variance explained. This lack of correlation may indicate air which has had NO_y removed. It could also reflect transport processes that deliver air with a higher natural ozone contribution. For example, we have identified at least two cases where enhanced ozone

concentrations are observed in the NW-fast PATH behind surface cold-frontal passages. Hourly O_3 in these events is anticorrelated with CO and occurs with subsiding trajectories and dry air at the surface, suggesting a contribution from stratospherically enhanced O_3 in the midtroposphere, consistent with the meteorological mechanism described by *Moody et al.* [1996].

There is uncertainty in the use of any of these statistical measures of ozone correlation (O_3 versus NO_z, O_3/CO, photochemical age), and it is important to acknowledge that factors such as surface uptake of O_3 and wet removal of NO_y may limit our ability to interpret these relationships. Nonetheless, a reasonably consistent picture emerges when these chemical relationships are considered together and when they are viewed in the context of air mass transport history and the potential differences in source region that different PATHs represent. Our results support the conclusions that O_3 is less correlated with NO_z in urban or unaged air masses (e.g., SW PATH) relative to rural or aged air masses (e.g., W PATH). We acknowledge it is also possible for the O_3 versus NO_z slope to increase not due to chemistry but as a result of NO_y removal (e.g., anticyclonic flow).

In an effort to further assess the events associated with enhanced summer O_3 mixing ratios, we looked at the subset of 3-hour averages when O_3 was greater than 50 ppb. In the summer months, 39% of the data met this criteria. When we analyzed this subset by PATH, it was apparent that a higher fraction of the westerly PATH, two thirds or 66%, had enhanced O_3. The majority of local PATH events (55%) also had enhanced O_3 concentrations during the summer. It was common for these enhanced O_3 averages to occur for subsequent days, with frequent transitions from the local PATH to the W PATH. These observations are consistent with the work of *Logan* [1989] which identified O_3 episodes at rural sites that were regional in scale, persisting for multiple days, and occurring under slow-moving high-pressure systems. Both the local and W PATH meteorological conditions are consistent with summer high-pressure systems. The fact that high O_3 was consistently observed under the W PATH is good evidence of the broad regional extent of these episodes.

4.2. Corroborating Source Regions

We have used the trajectory data to characterize patterns in atmospheric transport history and to illustrate that PATH does influence chemical concentrations. To corroborate these results, and assess the robustness of our conclusions, we have used the chemical data to describe the origin of (1) background air and (2) pollution episodes. We have used

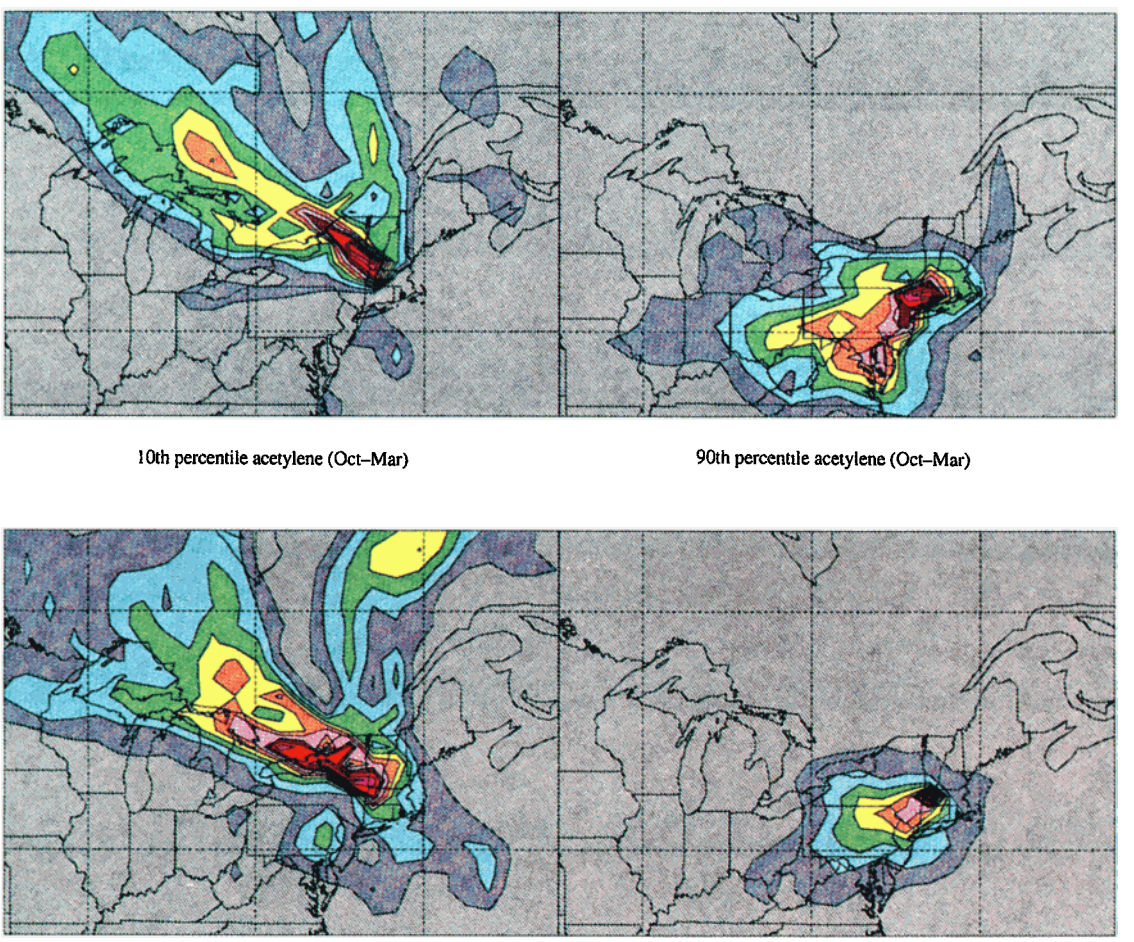

Plate 2. Probability plots showing the likelihood of transport from upwind regions using trajectories that correspond to the lowest 10% and the highest 90% of the acetylene mixing ratios in each season.

data representing extreme conditions, namely, the 10th and 90th percentiles of O_3, and acetylene mixing ratios. We use acetylene as an indicator of a relatively long-lived combustion-derived anthropogenic pollutant. Using all the chemical data, and splitting the year into warm and cool seasons, April-September and October-March, respectively, we have plotted the probability fields which illustrate the likelihood of trajectories having crossed upwind regions. Plate 2 shows the transport patterns of high and low acetylene by season. During the cool season, low values are associated with relatively strong winds from the NW, while high values of acetylene arrive from polluted East Coast source regions. In the warm season, the relative patterns are similar; however, we see the general shift to nearby sources having a higher probable contribution to 90th percentile events. This is due to the lower average wind speeds during the warm season and stagnant conditions resulting in acetylene accumulation.

For O_3 (Plate 3), we find that the lowest mixing ratios are associated with a transport path very similar to the one that delivered high anthropogenic pollution (e.g., acetylene) in the cool season. This illustrates that O_3 is lowest under conditions where it is depleted by fresh pollution. By contrast, the highest O_3 during the cool season appears to have a significant contribution from NW regions, under relatively high winds, and subsidence. This suggests that a significant portion of enhanced O_3 concentrations during the cool season may represent natural ozone exchanged into the free troposphere from the stratosphere. A secondary source region is suggested by flow from the SW. During the warm season, the lowest O_3 is associated with relatively clean transport from the NW or off the ocean, and the highest O_3 arrives under flow from the west, with the probability pattern suggestive of weak anticyclonic curvature, like a combination of the westerly and local flow PATHs.

5. Conclusions

We have demonstrated that the calculation of back trajectories to determine regional-scale patterns in atmospheric transport history (PATH) is an effective way of characterizing events which represent broadly similar synoptic conditions. We have shown that significantly different seasonal signals in trace gas concentrations are associated with different flow PATH. Our results indicate that N and NW-fast flow effectively characterize background conditions for the Harvard Forest site, with lower pollutant concentrations and lower variance observed under these transport PATHs. Anthropogenic pollutants (combustion-derived products) were highest under SW flow conditions, which were generally warm, moist, and relatively cloudy.

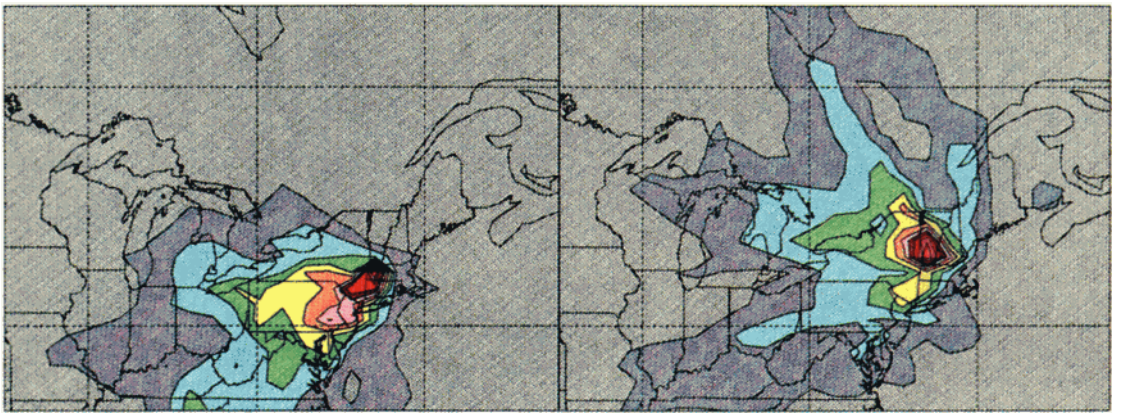

Plate 3. Probability plots showing the likelihood of transport from upwind regions using trajectories that correspond to the lowest 10% and the highest 90% of the ozone mixing ratios in each season.

This is indicative of warm sector transport. The highest O_3 concentrations did not occur under these conditions, which had a low O_3 production efficiency. Instead, the highest average summer O_3 occurred under W flow, which was generally very warm, and sunny, with the highest isoprene mixing ratios, and relatively dry air parcels associated with deep mixed layers and moderately strong wind speeds, which delivered well-aged air masses with high O_3 production efficiency. This implies an important contribution of advected pollutants from Midwest source regions under meteorological conditions which suggest an advancing ridge of high pressure. These general results are corroborated by plotting probability fields of 10th and 90th percentile concentrations for O_3 and the relatively long-lived anthropogenic hydrocarbon, acetylene.

There were insufficient data in this 4-year record to effectively analyze interannual variations in chemical composition. However, we anticipate that using a longer chemical/transport data record would provide us with an opportunity to asses the degree to which temporal trends in chemical concentrations of the NE (or other measures of interannual variation [*Goulden et al.*, 1996]) may be driven by changes in the frequency of occurrence of meteorological conditions from year to year.

Acknowledgments. This manuscript was supported by a grant from the Northeast Regional Center of the National Institute for Global Environmental Change (901214-HAR). Jennie L. Moody would like to thank Roland Draxler at NOAA/ARL for encouraging the development of the PATH model and providing assistance and data for adaptation of HYSPLIT; Jonathan Newbrough of the University of Virginia for rewriting and developing model code; Clay Davenport for technical assistance; and S. Sillman, University of Michigan; D. Fitzjarrald, SUNY-Albany; and W. C. Keene of UVA for helpful discussions on the analyses and text.

References

Chai, X., and V. A. Mohnen, Whiteface Mountain ozone and sulfate: An investigation of the background concentration representative for the northeastern United States, *Atmos. Environ.*, in press, 1998.

Chin, M., D. J. Jacob, J. W. Munger, D. D. Parrish, and B. G. Doddridge, Relationship of ozone and carbon monoxide over North America, *J. Geophys. Res.*, *99*, 14,565-14,573, 1994.

Dorling, S. R., T. D. Davies, and C. E. Pierce, Cluster analysis: A technique for estimating the synoptic meteorological controls on air and precipitation chemistry - Method and applications, *Atmos. Environ., Part A, 25*, 2575-2581, 1992.

Draxler, R. R., Hybrid single-particle Lagrangian integrated trajectories (HY-SPLIT): Version 3.0--User's guide and model description; *NOAA Tech. Memo ERL/ARL-195*, pp. 40, Natl. Oceanic and Atmos. Admin., Silver Spring, Md., 1992. (Available from Natl. Tech. Inf. Serv., Springfield, Va.

Goldstein, A. H., B. C. Daube, J. W. Munger, and S. C. Wofsy, Automated in situ monitoring of atmospheric nonmethane hydrocarbon concentrations and gradients, *J. Atmos. Chem.*, *21*, 43-59, 1995a.

Goldstein, A. H., S. C. Wofsy, and C. M. Spivakovsky, Seasonal variations of nonmethane hydrocarbons in rural New England: Constraints on OH concentrations in northern midlatitudes, *J. Geophys. Res.*, *100*, 21,023-21,033, 1995b.

Goulden, M. L., J. W. Munger, S.-M. Fan, B. C. Daube, and S. C. Wofsy, Exchange of carbon dioxide by a deciduous forest: Response to interannual climate variability, *Science, 271*, 1576-1578, 1996.

Harris, J. M., and J. D. Kahl, A descriptive atmospheric transport climatology for the Mauna Loa Observatory using clustered trajectories, *J. Geophys. Res.*, *95*, 13,651-13,667, 1990.

Hirsch, A. I., J. W. Munger, D. J. Jacob, L. W. Horowitz, and A. H. Goldstein, Seasonal variation of the ozone production efficiency per unit NO_x at Harvard Forest, Massachusetts, *J. Geophys. Res.*, *101*, 12,659-12,666, 1996.

Hoke, J.E., N. A. Philips, G. J. DiMego, J. J. Tucillo, and J. G. Sela, The regional analysis and forecast system of the National Meteorological Center, *Weather Forecasting*, *4*, 323-334, 1989.

Holzworth, G. C., Mixing depths, wind speeds and air pollution potential for selected locations in the United States, *J. Appl. Meteorol.*, *6*, 1039-1044, 1967.

Jacob, D. J., L. W. Horowitz, J. W. Munger, B. G. Heikes, R. R. Dickerson, R. S. Artz, and W. C. Keene, Seasonal transition from NO_x- to hydrocarbon-limited ozone production over the eastern United States in September, *J. Geophys. Res.*, *100*, 9315-9324, 1995.

Kleinman, L., et al., Ozone formation at a rural site in the southeastern United States, *J. Geophys. Res.*, *99*, 3469-3482, 1994.

Lin, X., M. Trainer, and S. C. Liu, On the nonlinearity of the tropospheric ozone production, *J. Geophys. Res.*, *93*, 15,879-15,888, 1988.

Logan, J. A., Ozone in rural areas of the United States, *J. Geophys. Res.*, *94*, 8511-8532, 1989.

McKeen, S. A., E.-Y. Hsie, M. Trainer, R. Tallamraju, and S. C. Liu, A regional model study of the ozone budget in the eastern United States, *J. Geophys. Res.*, *96*, 10,809-10,845, 1991.

Moody, J. L., and J. N. Galloway. Quantifying the relationship between atmospheric transport and the chemical composition of precipitation on Bermuda, *Tellus, Ser B, 40*, 463-479, 1988.

Moody, J. L., and P. J. Samson, The influence of atmospheric transport on precipitation chemistry at two sites in the midwestern United States, *Atmos. Environ.*, *23*, 2117-2132, 1989.

Moody, J. L., S. J. Oltmans, H. Levy II, and J. T. Merrill, Transport climatology of tropospheric ozone: Bermuda, 1988-1991, *J. Geophys. Res.*, *100*, 7179-7194, 1995.

Moody, J. L., J. C. Davenport, J. T. Merrill, S. J. Oltmans, D. D. Parrish, J. S. Holloway, H. Levy II, G. L. Forbes, M. Trainer, and M. Buhr, Meteorological mechanisms for transporting O_3 over the western North Atlantic Ocean: A case study for August 24-29, 1993, *J. Geophys. Res.*, *101*, 29,213-29,228,1996.

Moore, K. E., D. R. Fitzjarrald, R. K. Sakari, M. L. Goulden, J. W. Munger, and S. C. Wofsy, Seasonal variation in radiative and turbulent exchange at a deciduous forest in central Massachusetts, *J. Appl. Meteorol*, *35*, 122-134, 1996.

Moy, L. A., R. R. Dickerson, and W. F. Ryan, How meteorological conditions affect tropospheric trace gas concentrations in rural Virginia, *Atmos. Environ.*, *28*, 2789-2800, 1994.

Munger, J. W., S. C. Wofsy, P. S. Bakwin, S.-M. Fan, M. L. Goulden, B. C. Daube, and A. H. Goldstein, Atmospheric deposition of reactive nitrogen oxides and ozone in a temperate deciduous forest and a sub-Arctic woodland, 1, Measurements and mechanisms, *J. Geophys. Res.*, *101*, 12,639-12,658, 1996.

Olszyna, K. J., E. M. Baily, R. Simonaitis, and J. F. Meagher, O_3 and NO_y relationships at a rural site, *J. Geophys. Res.*, *99*, 14,557-14,563, 1994.

Oltmans, S. J., and H. Levy II, Surface ozone measurements from a global network, *Atmos. Environ.*, *28*, 9-24, 1994.

Parrish, D. D., J. S. Holloway, M. Trainer, P. C. Murphy, G. L. Forbes, and F. C. Fehsenfeld, Export of North American ozone pollution to the North Atlantic Ocean, *Science*, *259*, 1436-1439, 1993.

Parrish, D. D., M. Trainer, J. S. Holloway, J. E. Yee, M. S. Warshawsky, F. C. Fehsenfeld, G. Forbes, and J. L. Moody, Relationship between ozone and carbon monoxide at surface sites in the North Atlantic region, *J. Geophys. Res.*, in press, 1998.

Samson, P. J., and J. L. Moody, Backward trajectories as two-dimensional probability fields, in *Air Pollution Modeling and Its Applications, vol. 1*, pp. 43-54, Plenum, New York, 1981.

Sillman, S., J. A. Logan, and S. C. Wofsy, The sensitivity of ozone to nitrogen oxides and hydrocarbons in regional ozone episodes, *J. Geophys. Res.*, *95*, 1837-1852, 1990.

Sirois, A., and J. W. Bottenheim, Use of backward trajectories to interpret the 5-year record of PAN and O_3 ambient air concentrations at Kejimkujik National Park, Nova Scotia, *J. Geophys. Res.*, *100*, 2867-2881, 1995.

Trainer, M., et al., Correlation of ozone with NO_y in photochemically aged air, *J. Geophys. Res., 98, 2917-2925,* 1993.

Wofsy, S. C., M. L. Goulden, J. W. Munger, S.-M. Fan, P. S. Bakwin, B. C. Daube, S. L. Bassow, and F. A. Bazzaz, Net exchange of CO_2 in a mid-latitude forest, *Science, 260,* 1314-1317, 1993.

A. H. Goldstein, Environmental Science, Policy, and Management, University of California, Berkeley, CA 94720.

D. J. Jacob and J. W. Munger, Division of Applied Science, Harvard University, Cambridge, MA 02138.

J. L. Moody, Department of Environmental Sciences, University of Virginia, Charlottesville, VA 22903. (e-mail: moody@virginia.edu)

S. C. Wofsy, Northeast Regional Center, NIGEC, Harvard University, Cambridge, MA 02138.

(Received July 11, 1997; revised December 22, 1997; accepted February 12, 1998.)